Article

Preparation and Application of CO₂-Resistant Latex in Shale Reservoir Cementing

Chunyuan Jiang [1,2], Xuecheng Zheng [1,2,*], Yuanqiang Zhu [1,2], Lei Tang [3], Yuhao Liu [4], Zhijun Zhao [5] and Hongyu Zhang [6]

1 College of Chemistry and Chemical Engineering, Southwest Petroleum University, Chengdu 610500, China
2 Oil & Gas Field Applied Chemistry Key Laboratory of Sichuan Province, Chengdu 610500, China
3 Sichuan Ruidong Technology Co., Ltd., Chengdu 610500, China
4 CNPC Chuanqing Drilling Engineering Company Ltd., Chengdu 610066, China
5 Zhundong Drilling Company, CNPC Xibu Drilling Engineering Company Ltd., Changji 831199, China
6 College of Engineering, Southwest Petroleum University, Nanchong 637001, China
* Correspondence: xc.zheng@swpu.edu.cn

Abstract: With the application of CO_2 fracturing, CO_2 huff and puff, CO_2 flooding, and other stimulation technologies in shale reservoirs, a large amount of CO_2 remained in the formation, which also lead to the serious corrosion problem of CO_2 in shale reservoirs. In order to solve the harm caused by CO_2 corrosion, it is necessary to curb CO_2 corrosion from the cementing cement ring to ensure the long-term stable exploitation of shale oil. Therefore, a new latex was created using liquid polybutadiene, styrene, 2-acrylamide-2-methylpropanesulfonic acid, and maleic anhydride to increase the cement ring's resistance to CO_2 corrosion. The latex's structure and characteristics were then confirmed using infrared, particle size analyzer, thermogravimetric analysis, and transmission electron microscopy. The major size distribution of latex is between 160 and 220 nm, with a solid content of 32.2% and an apparent viscosity of 36.8 mPa·s. And it had good physical properties and stability. Latex can effectively improve the properties of cement slurry and cement composite. When the amount of latex was 8%, the fluidity index of cement slurry was 0.76, the consistency index was 0.5363, the free liquid content was only 0.1%, and the water loss was reduced to 108 mL. At the same time, latex has a certain retarding ability. With 8% latex, the cement slurry has a specific retarding ability, is 0.76 and 0.5363, has a free liquid content of just 0.1%, and reduces water loss to 108 mL. Moreover, latex had certain retarding properties. The compressive strength and flexural strength of the latex cement composite were increased by 13.47% and 33.64% compared with the blank cement composite. A long-term CO_2 corrosion experiment also showed that latex significantly increased the cement composite's resilience to corrosion, lowering the blank cement composite's growth rate of permeability from 46.88% to 19.41% and its compressive strength drop rate from 27.39% to 11.74%. Through the use of XRD and SEM, the latex's anti-corrosion mechanism, hydration products, and microstructure were examined. In addition to forming a continuous network structure with the hydrated calcium silicate and other gels, the latex can form a latex film to attach and fill the hydration products. This slows down the rate of CO_2 corrosion of the hydration products, enhancing the cement composite's resistance to corrosion. CO_2-resistant toughened latex can effectively solve the CO_2 corrosion problem of the cementing cement ring in shale reservoirs.

Keywords: shale reservoirs; supercritical CO_2; well cementing; styrene–butadiene latex; CO_2 corrosion; working mechanism

1. Introduction

The current research gradually focuses on the development of unconventional oil and gas resources, particularly the development of shale oil resources [1,2], as a result of the growing demand for oil and gas resources in social development and the significantly declining amount of exploitable conventional reservoir resources. At present, shale

reservoirs frequently used formation fracturing techniques to boost output. However, the fracturing pressure of conventional fracturing methods decreased rapidly, and the pressure cannot be transferred to the tight formation, resulting in the formation of fractures and the limited production effect in shale reservoirs. Thus, more CO_2-fracturing technology was employed for the development of unconventional oil reserves like shale reservoirs. CO_2 may go from a gas to a supercritical state and persist steadily in an environment where the temperature and pressure are both higher than 31.1 °C and 7.38 MPa. CO_2 may go from a gas to a supercritical state and persist steadily in an environment where the temperature and pressure were both higher than 31.1 °C and 7.38 MPa. Supercritical CO_2 had both the flow characteristics of liquid and the flow resistance of gas, so that CO_2 can effectively spread the micro pores and channels in the formation under the push of fracturing pressure. And supercritical CO_2 can continue to exert osmotic pressure on the micro pores, so as to achieve the purpose of efficient fracturing, so as to improve the production of shale oil. On the basis of CO_2 fracturing, CO_2 can also be used for CO_2 huff and huff, CO_2 flooding, and other stimulation methods to promote the development and utilization of shale reservoirs [3–5].

Due to the influence of the anisotropic strength properties of shale [6–8], it was easy to cause formation instability with organic rich shales, which required improving the cementing quality. We minimize the impact of shale instability and guarantee the integrity of the wellbore in shale reservoirs. Meanwhile, utilizing CO_2 can promote the development rate of the shale reservoir, but it will also increase the corrosion of CO_2 on the cement ring. CO_2 corrosion usually occurred in the formation with a high CO_2 content, and the development of CO_2 injection into the oil well created the corresponding conditions for CO_2 corrosion on the cement ring. The hydration products created by cement will cause the CO_2 in the formation to undergo a number of chemical corrosion processes, including leaching, decalcification, carbonization, and dissolution. The CO_2 in the supercritical state, which was more likely to corrode through the pores or cracks of the cement ring, will erode the alkaline substances in the cement ring through a series of chemical corrosion reactions that include leaching, decalcification, carbonization, and dissolution with the hydration products formed by the cement [9,10]. The complete CO_2 oxidation of the cement ring resulted in the loss of the cement ring's suspending effect on the cementing casing and the formation fluid's cross-flow, which posed a risk of working fluid pollution, formation damage, and the corrosion of the pipes [11,12]. Consequently, in order to lessen the damage caused by CO_2 corrosion and increase the service life of shale oil wells, efficient measures to increase the corrosion resistance of cement rings must be taken.

Numerous studies have demonstrated that the present focus on developing shale reservoirs mostly concentrates on using CO_2 for development and stimulation [13–16], with little regard for the corrosion risks that CO_2 poses to oil wells. Therefore, in order to prevent more CO_2-corrosion-related damage to oil wells, prompt action must be taken to address the issue of CO_2 corrosion on cementing cement ring. At present, the corrosion resistance of cement was mainly improved by improving the composition of the cement system, increasing the density of the cement composite and providing a protective layer for the cement composite. Among them, the more effective measures were adding cement admixtures, anti-corrosion materials, anti-corrosion admixtures, or anti-corrosion coatings to the cement slurry system. Morandeau et al. [17] studied the effect of fly ash on the corrosion resistance of the cement composite, and the experiment showed that the decline in the compressive strength of the cement composite could be effectively slowed down when the amount of fly ash was more than 30%. Gong et al. [18] used calcium aluminate cement to improve the integrity of cement rings in a CO_2 environment. Compared with ordinary Portland cement, calcium aluminate cement can better cope with CO_2 corrosion in the formation, and the corrosion rate of calcium aluminate cement is slower. Peng et al. [19] modified the traditional oil-based epoxy resin with a high-temperature-resistant monomer to obtain an anticorrosive epoxy resin, which greatly improved the anticorrosive performance of the epoxy resin in the oil well cement. Zhang et al. [20] solved the problem

of the poor dispersion and low stability of epoxy resin in the cement slurry, and this resin can effectively improve the compressive strength of the cement composite after curing and the decline in compressive strength after CO_2 corrosion. Wang et al. [21] found that adding a small amount of styrene–butadiene latex to the cement slurry can effectively improve the mechanical properties of the cement composite, and found that the influence of latex on the cement composite formed a continuous structure with the polymer film formed by latex and cement hydration products. Wang et al. [22] synthesized modified polyacrylate latex with methyl methacrylate and butyl acrylate. This latex can gradually hydrolyze the ester group of the molecular chain into a carboxylic group in an alkaline environment, and better $Ca(OH)_2$ can be cemented to form a network structure. Faruk et al. [23] compared the performance of styrene–butadiene latex and styrene–propyl latex in the process of CO_2 corrosion. Styrene–butadiene latex has a stronger performance in improving the cement slurry, and styrene–butadiene latex has a stronger polymer-film-forming performance and stronger carbonization resistance, which is more suitable for improving the corrosion resistance of the cement composite.

By comparing various methods to improve the corrosion resistance of the cement ring, styrene–butadiene latex was an excellent material to improve the corrosion resistance of the cementing cement ring. It can not only improve the corrosion resistance of the cementing cement ring, but also improve the strength and toughness of the cement ring, reduce the damage of the cement ring during the fracturing development of the shale reservoir, and reduce the strength decline of the cement ring. However, there has not been enough research carried out on styrene–butadiene latex to address CO_2 corrosion in the cement rings as of yet. Therefore, a new kind of CO_2-resistant toughened latex was synthesized and analyzed using liquid polybutadiene, styrene, 2-acrylamide-2-methylpropanesulfonic acid, and maleic anhydride. The research examined the effect of latex on the performance of the cement slurry system, the improvement of the anti-CO_2 corrosion performance of the system and the anti-corrosion mechanism of latex. The improvement effect of CO_2-corrosion-resistant toughened rubber latex on the corrosion resistance of the cement ring was deeply explored, and the CO_2 corrosion harm caused by CO_2 exploitation in the shale reservoir was solved.

2. Experiments

2.1. Materials and Equipment

The materials and equipment were shown in Tables 1 and 2. The chemical composition of G class oil well cement was shown in Table 3. All of these were commercial products and used without further purification.

Table 1. Materials and related information.

Materials	Chemical Purity	Manufacturer
Liquid polybutadiene (PB)	Average Mn 1530–2070	Chengdu Huaxia Chemical Reagent Co., Ltd.
Styrene (St)	CP	Chengdu Colon Chemical Co., Ltd.
2-acrylamide-2-methylpropanesulfonic acid (AMPS)	AR	Chengdu Huaxia Chemical Reagent Co., Ltd.
Maleic anhydride (MA)	AR	Shanghai Maclin Biochemical Technology Co., Ltd.
Sodium dodecyl sulfate (SDS)	AR	Chengdu Colon Chemical Co., Ltd.
Ammonium persulfate (APS)	GR	Chengdu Colon Chemical Co., Ltd.
Sodium hydroxide (NaOH)	GR	Chengdu Colon Chemical Co., Ltd.
Calcium chloride ($CaCl_2$)	GR	Chengdu Colon Chemical Co., Ltd.
Sodium chloride (NaCl)	GR	Chengdu Colon Chemical Co., Ltd.
Magnesium chloride ($MgCl_2$)	GR	Chengdu Colon Chemical Co., Ltd.
G class oil well cement	Technical grade	Jiahua Special Cement Co., Ltd.
Micro-silicon	Technical grade	Sichuan Zhengrong Industrial Co., Ltd.

Table 1. *Cont.*

Materials	Chemical Purity	Manufacturer
Fluid loss additive	Technical grade	Tianjin Boxing Engineering Technology Co., Ltd.
Dispersant	Technical grade	Weihui Chemical Co., Ltd.
Defoamer	Technical grade	Client supply
Pure water	Primary purified water	Tianjin development zone ruier environmental protection Technology Co., Ltd.
Carbon dioxide	99.999	Chengdu Xindu District Zhengrong gas Co., Ltd.
Nitrogen	99.999	Chengdu Xindu District Zhengrong gas Co., Ltd.
Phenolphthalein	Ph Eur., 98%	Shijiazhuang Simo Technology Co., Ltd.

Table 2. Experimental equipment.

Equipment	Manufacturer
Stainless steel masher	Shanghai Jingke Industrial Co., Ltd.
WQF-520 infrared spectrometer	Beijing Ruili Analytical Instrument Co., Ltd.
Talos F200S G2 S transmission electron microscope	Thermo Fisher Technologies Ltd.
Zeta potential and nano-size analyzer	Malvern Panalytical Instruments Ltd.
TGA 2 thermogravimetric analyzer	Mettler Toledo International Trading Co. Ltd.
NDJ-79 rotational viscometer	Shanghai Fangrui Instrument Co., Ltd., China
X-ray diffractometer	Dutch Panaco Company
Quanta 650 Field Emission Scanning Electron Microscope	FEI Czech Republic S. r. o
High-temperature and high-pressure CO_2-curing kettle	Self-innovate
Cement stone strength test mold	Self-innovate
Hydraulic servo drive control universal testing machine	Mets Industrial Systems (China) Co., Ltd.
Energy-Dispersive X-ray Spectroscopy	Shimadzu Corporation of Japan
Laboratory ultrapure water equipment	Shijiazhuang Simo Technology Co., Ltd.

Table 3. Chemical composition of G class oil well cement, wt%.

SiO_2	Al_2O_3	Fe_2O_3	MgO	CaO	K_2O	Na_2O	SO_3	Others
22.31	3.60	4.76	1.29	64.06	0.41	1.48	0.96	1.13

2.2. Experimental Methods

2.2.1. Synthesis and Property Analysis of CO_2-Resistant Latex

In order to guarantee that the produced latex had high qualities and particle size, seed emulsion polymerization was used to create CO_2-corrosion-resistant latex, and the semi-continuous technique of latex monomer addition was used [24]. Figures 1 and 2 depicted the synthesis reaction and the process of experimentation. The synthesis steps were as follows: after thoroughly mixing LPB, St, and SDS into nuclear emulsion A, and MA, AMPS, and APS into shell monomer solution B, they were each given a 30 min stir. After that, the flask was filled with the required amounts of nuclear emulsion A and shell monomer solution B, and it was heated to 75 °C in the oil bath. Initiate the agitator and set the stirring rate to 250 rpm. Inject nitrogen continually and let it react for one hour to make the seed emulsion. Following the preparation of the seed emulsion, the leftover solution A and solution B were added to the constant-pressure falling funnel, respectively, and allowed to react steadily for two hours. The CO_2-resistant toughened latex was obtained by allowing the reaction to proceed for three hours after the drop was introduced.
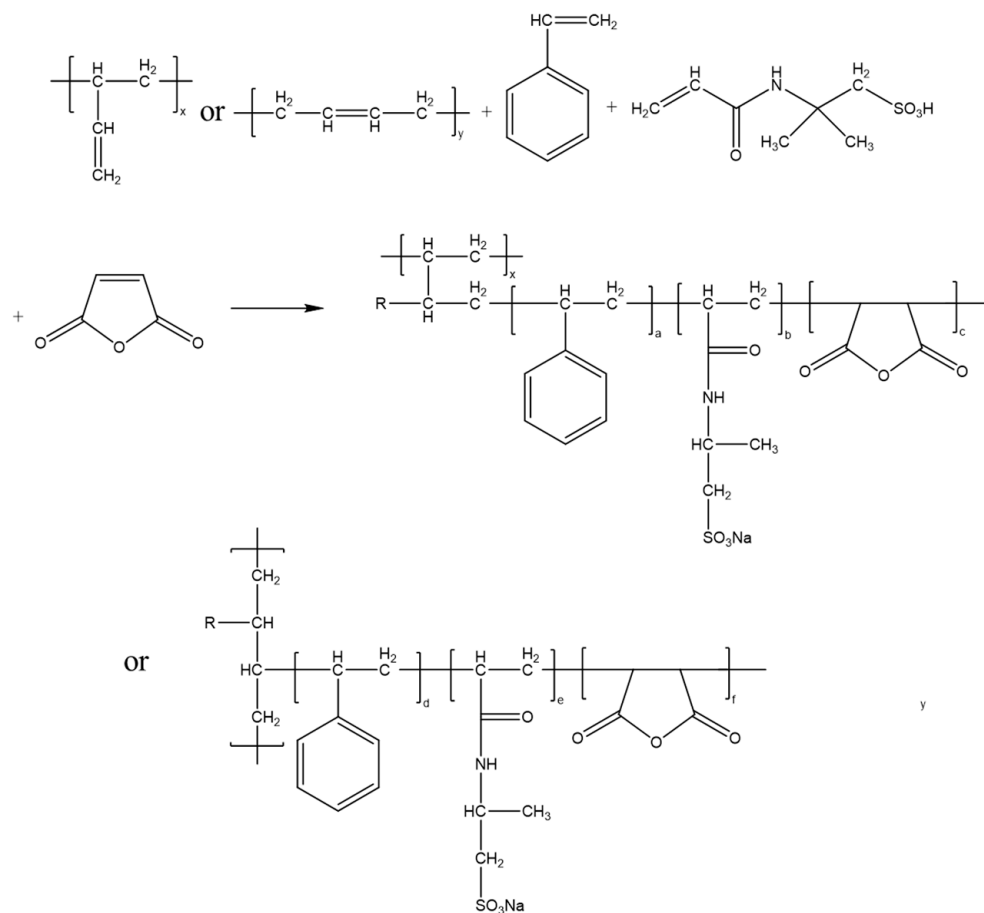
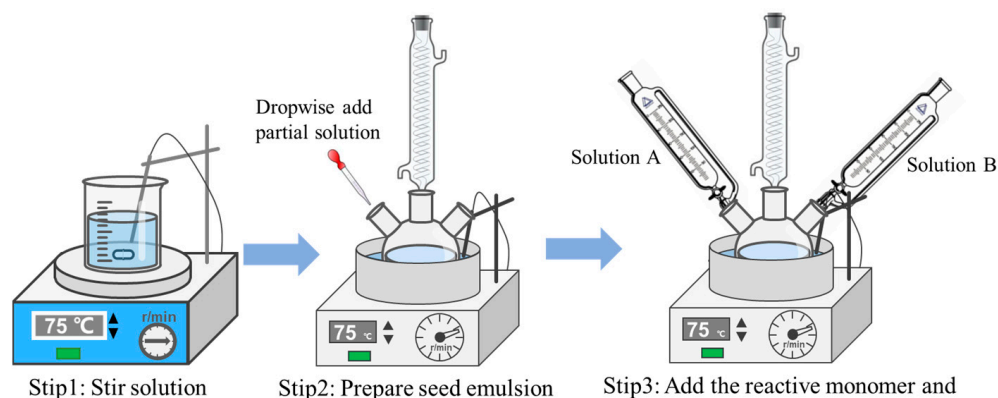**Figure 1.** Synthesis formula of CO_2-resistant toughened latex.

Figure 2. Experimental flow chart of synthetic latex.

The research began with an examination of the CO_2-resistant toughened latex's molecular structure, temperature resistance, and particle size distribution. FTIR was used to measure the infrared spectrum of latex at 4000–400 cm^{-1}. The particle size distribution of latex was analyzed by DLS. The temperature stability of latex was analyzed by TGA. The core-shell structure and particle size of latex particles were observed by TEM. EDX was used to observe the elemental changes of cement.

The latex's mechanical stability, salt resistance stability, freeze–thaw stability, and physical characteristics were next analyzed. The apparent viscosity of latex was determined by a rotary viscometer. The quality change of latex before and after complete drying was measured by drying method to obtained the solid content of latex. The mechanical stability experiment was to stir the latex at 3000 rpm for 5 min, and then carry out constant-pressure

pumping and filtering, so that the latex particles generated by mechanical agitation are attached to the filter paper. When the mass fraction of the mass change of the filter paper to the total mass of the original latex was less than 0.2%, the mechanical stability of the latex was good. The salt stability test was conducted by adding saturated $CaCl_2$, NaCl, and $MgCl_2$ solutions to the latex drops. If the latex did not break or flocculate, the salt stability of the latex is good [25]. Similarly, the freeze–thaw stability experiment was a freeze–thaw cycle in which the latex is frozen at −20 °C for 18 h, and then thawed naturally at 25 °C for 6 h. The cycle was carried out until the latex cannot recover its initial state, and the number of 7 cycles was recorded. When the number of cycles was greater than 4 times, the freeze–thaw stability was good [26].

2.2.2. Experiment on the Effect of Latex on the Properties of Cement Slurry

In order to explore the effect of CO_2-resistant toughened latex on the system, the formula of the cement slurry was designed as shown in Table 4. The prepared cement blocks were compressive strength test molds (diameter 25 mm × height 50 mm) and flexural strength test molds (length 40 mm × width 40 mm × height 100 mm), and the preparation process of cement slurry and cement blocks was carried out according to the American Petroleum Institute (API). Concurrently, the effect of the amount of latex on the rheology, stability, and thickening process of cement slurry, as well as the physical strength and microstructure of cement were investigated.

Table 4. Composition ratio of cement slurry, g.

Sample	Cement	Micro-Silicon	Fluid Loss Additive	Dispersant	Latex	Defoamer	Water
1	600	24	0	0	0	3	264
2	600	24	0	0	24	3	264
3	600	24	0	0	48	3	264
4	600	24	0	0	72	3	264

2.2.3. CO_2 Corrosion Test of Latex Cement Composite

The compressive strength test mold was prepared according to the specified process of API, and was cured in a water bath environment of 90 °C and 15 MPa for 7 days. Following the curing period, the cement composite was moved to a high-temperature and high-pressure CO_2-curing kettle, and the CO_2 corrosion test was conducted in accordance with the procedure depicted in Figure 3. In order to investigate the enhancement effect of the CO_2-resistant toughened latex on the corrosion resistance of the system and the anti-corrosion mechanism of the latex, the cement should be corroded at 90 °C and 15 MPa for 60 days in the CO_2 liquid-phase corrosion environment. After 0, 20, 40, and 60 days of CO_2 corrosion, the physical properties and physical composition of different cement composite were analyzed to explore the improvement effect of CO_2-resistant toughened latex on the corrosion resistance of the system and the anti-corrosion mechanism of the latex. The formula of cement slurry was shown in Table 5.

Table 5. Composition ratio of cement slurry in CO_2 corrosion, g.

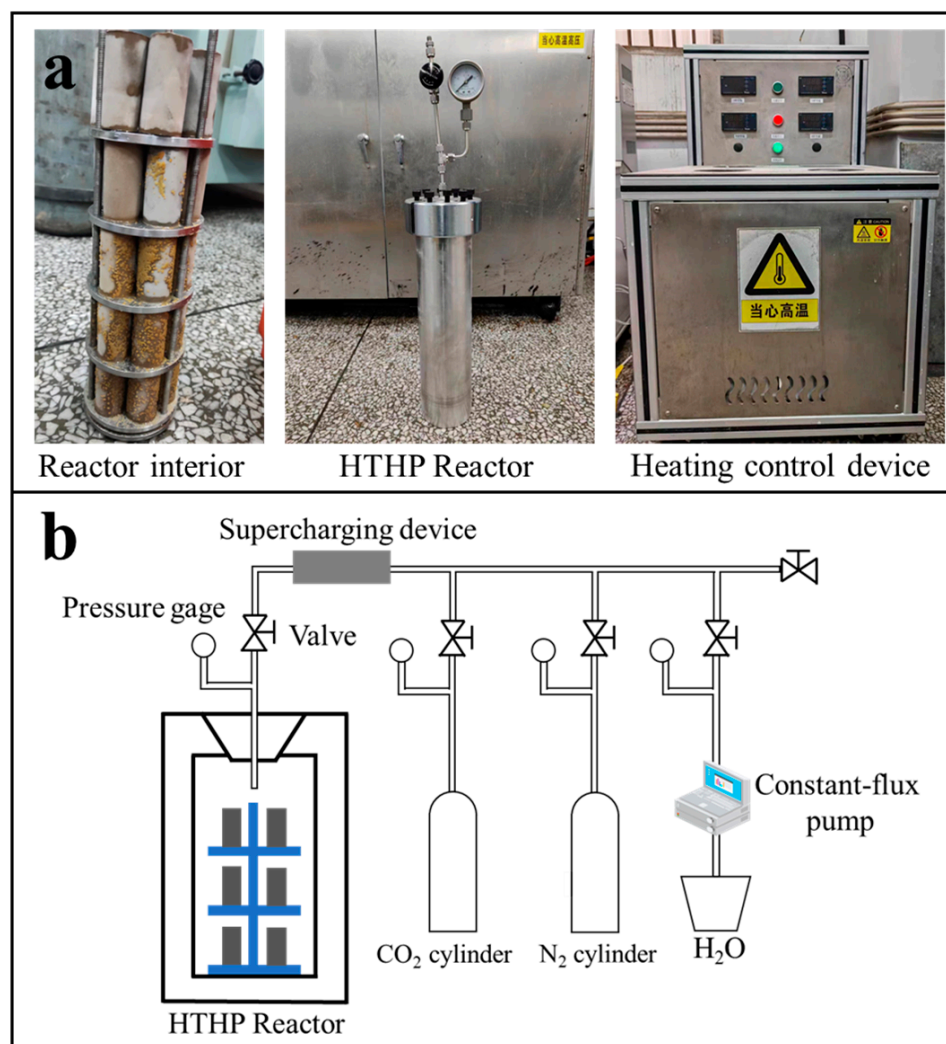| Sample	Cement	Micro-Silicon	Fluid Loss Additive	Dispersant	Latex	Defoamer	Water
L0	600	24	18	3	0	3	264
L4	600	24	18	3	24	3	264
L8	600	24	18	3	48	3	264
L12	600	24	18	3	72	3	264

Figure 3. Experimental flow chart of CO_2 corrosion cement ((**a**). Corrosion device components, and (**b**). Corrosion device schematic diagram).

3. Results and Discussion

3.1. Structure and Properties of CO_2-Resistant Toughened Latex

3.1.1. FTIR Analysis

According to the infrared spectrum test results in Figure 4, it can be found that the strong absorption peak at 3416 cm^{-1} came from the N-H bond connected with C=O in AMPS. The absorption peak at 3060 cm^{-1} was the -CH absorption peak of olefin. The absorption peak at 3026 cm^{-1} was produced by C-H connected to the benzene ring. The absorption peak at 2924 cm^{-1} was -CH$_2$. The absorption peak at 1719 cm^{-1} was the stretching vibration peak of -COOH in maleic anhydride. The absorption peak at 1640 cm^{-1} was the characteristic peak of the AMPS amide bond. The absorption peaks at 1551 cm^{-1}, 1493 cm^{-1}, 1453 cm^{-1}, and 1391 cm^{-1} were the stretching vibration peaks of the conjugated system formed by the benzene ring and maleic anhydride. The absorption peaks at 1186 cm^{-1} and 1055 cm^{-1} were the symmetric and asymmetric stretching vibration peaks of the sulfonic acid group S=O in AMPS. The absorption peaks at 697 cm^{-1} and 623 cm^{-1} were the stretching vibration peaks of the benzene ring single substitution. It can be seen that the synthesized latex contained all the characteristic structures of the reaction monomer, and the CO_2-corrosion-resistant toughened latex was successfully synthesized.
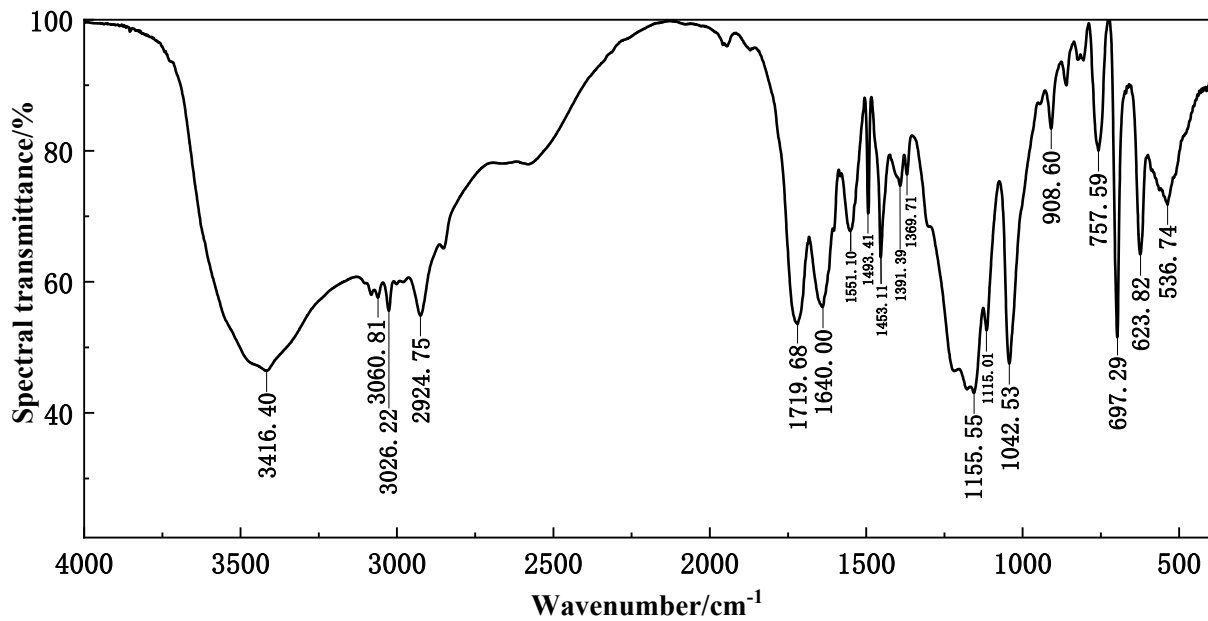
Figure 4. FTIR spectrum of CO_2-resistant toughened latex.

3.1.2. DLS Analysis

Figure 5 illustrated the particle size distribution of the latex. CO_2-resistant toughened latex had a particle size distribution ranging from 50 nm to 500 nm, with a predominant distribution between 160 nm and 220 nm. The latex's average particle size was 208.5 nm, which suggested that it had large-enough particles to accomplish the desired result.
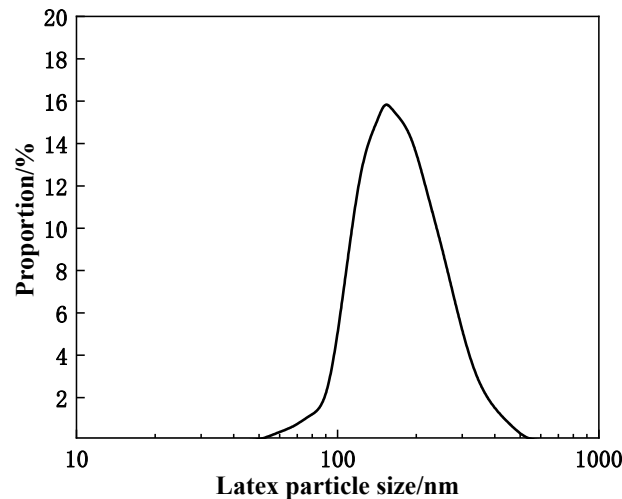

Figure 5. Size distribution of CO_2-resistant toughened latex.

3.1.3. TGA Analysis

Figure 6 illustrated the thermogravimetric spectrum of the CO_2-resistant toughened latex. It can be seen that, when the temperature of the thermal analysis was less than 25 °C, a small amount of decomposition occurs in the latex, and its mass fraction was reduced by 6.4%. In this process, the decomposition occurred mainly in the copolymer attached to the main chain of the latex or the part with a low polymerization degree. When the temperature exceeded 300 °C, a large amount of latex decomposition occurred, and the main thing that occurred in this process was the break and decomposition of the main chain of latex molecules, which made the latex decompose rapidly until the temperature reached 460 °C, and the quality of latex was lost by 81.4%. When the temperature exceeded

460 °C, the decomposition of benzene ring mainly occurred, and the mass loss was small. The results showed that the CO_2-resistant toughened latex had a high-molecular-weight stability and it was not easy to break and decompose molecular chains at 300 °C, which indicated that the CO_2-resistant toughened latex had good temperature stability.
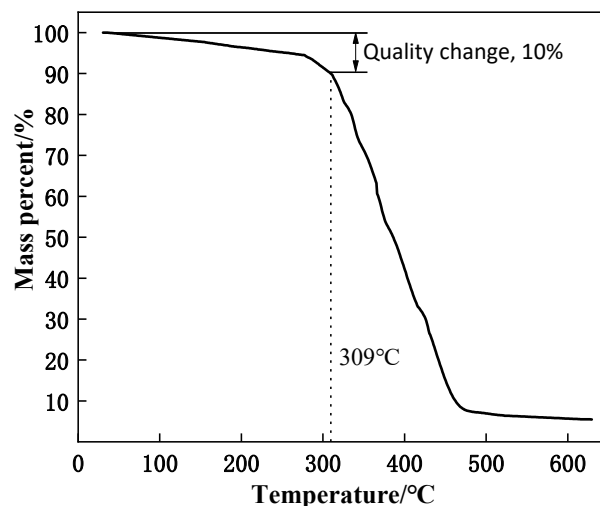

Figure 6. Thermogravimetric spectrum of CO_2-resistant toughened latex.

3.1.4. TEM Analysis

The transmission electron microscopy of the CO_2-corrosion-resistant toughened latex's particle structure was displayed in Figure 7. The preceding figure showed that the particle size distribution was focused and that the majority of latex particles may be kept in the 160–200 nm range. The figure demonstrated the clear core-shell structure of the latex and the uniform dispersion of the latex particles in the solution.
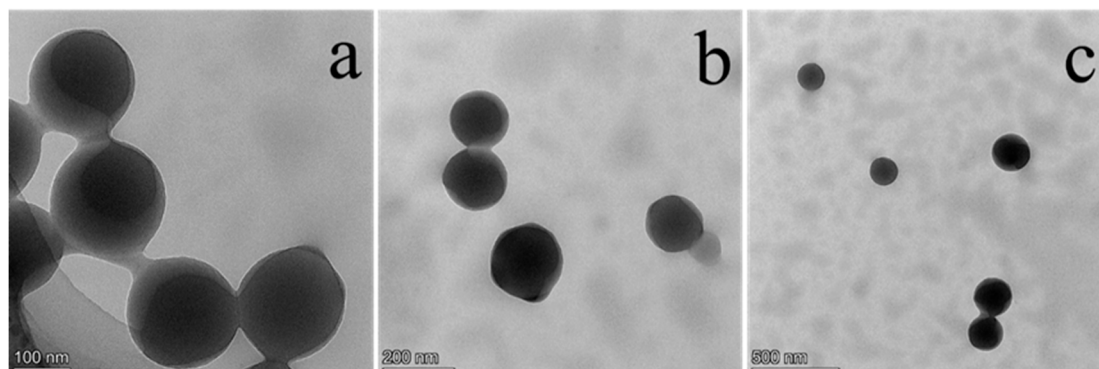

Figure 7. TEM image of CO_2-resistant toughened latex ((**a**). 100 nm, (**b**). 200 nm, and (**c**). 500 nm).

3.1.5. Performance Analysis of Latex

The physical characteristics and stability of both the regular styrene–butadiene latex and CO_2-resistant toughened latex were ascertained through a series of studies. Table 6 displayed the physical characteristics of CO_2-resistant toughened latex. The latex had the same physical characteristics as traditional styrene–butadiene latex and showed a strong long-term stability.

Table 7 showed the chemical composition of the CO_2-resistant toughened latex, in which PB and St were the core structure of the latex, and the higher content can ensure the good rigidity and mechanical stability of the latex. AMPS and MA as the shell structure of the latex can further improve the temperature resistance and film-forming ability of the latex; SDS can promote the stability of the latex; and NaCl and APS were the raw materials of the latex synthesis (Table 8).

Table 6. Physical properties of CO2-resistant toughened.

Physical Properties	Parameter
Appearance	Milky solution
pH	7~8
Solid content	32.2
Apparent viscosity, mPa·s	36.8
Free water content (20 °C ± 2 °C, 1 MPa), %	0
Long-term stability	No latex particles were produced

Table 7. Chemical composition of CO_2-resistant toughened latex, molar ratio.

PB	St	AMPS	MA	SDS	NaCl	APS
48.997	31	10	10	0.001	0.001	0.001

Table 8. Comparison of salt stability between CO_2-resistant toughened latex and ordinary latex.

Types of Latex	NaCl	$CaCl_2$	$MaCl_2$
CO_2-resistant toughened latex	No floccule	No floccule	No floccule
Ordinary latex	No floccule	Floccule 0.23 g	Floccule 0.31 g

Figure 8, Tables 8 and 9 demonstrated that the CO_2-resistant toughened latex can withstand multiple freeze–thaw cycles, high temperatures, high speed shear, saturated salt water, and other extreme environments without experiencing aberrant behaviors like flocculation. The findings demonstrated that, in terms of mechanical stability, temperature stability, salt stability, and freeze–thaw stability, CO_2-resistant toughened latex performed better than regular styrene–butadiene latex.

Figure 8. Flow state of latex after repeated freezing and thawing.

Table 9. Comparison of stability between CO_2-resistant toughened latex and ordinary latex.

Test Item	CO₂-Resistant Toughened Latex	Ordinary Latex
Mechanical stability	Mass change 0.1%	Mass change 0.6%
Temperature stability	Decomposition temperature > 309 °C	Decomposition temperature > 200 °C
Salt stability	No floccule	Floccule 0.31 g
Freeze–thaw stability	Freeze–thaw index ≥ 5	Freeze–thaw index ≤ 1

3.2. Effect of Latex on Properties of Cement Slurry and Cement Composite

3.2.1. Effect of Latex on the Properties of Cement Slurry

According to the results of the effect of the latex addition on the rheological properties of the latex cement in Figure 9, it can be seen that, with the increase in the latex addition, the fluidity index kept increasing, and the consistency index also decreased accordingly. A higher dispersion of the cement slurry [27,28] indicated that latex particles can fill between cement particles and act as ball-bearing lubrication [29]. When the amount of latex is 8%, the cement slurry was 0.76 and 0.5363, indicating that the latex can promote the rheology of the cement slurry.
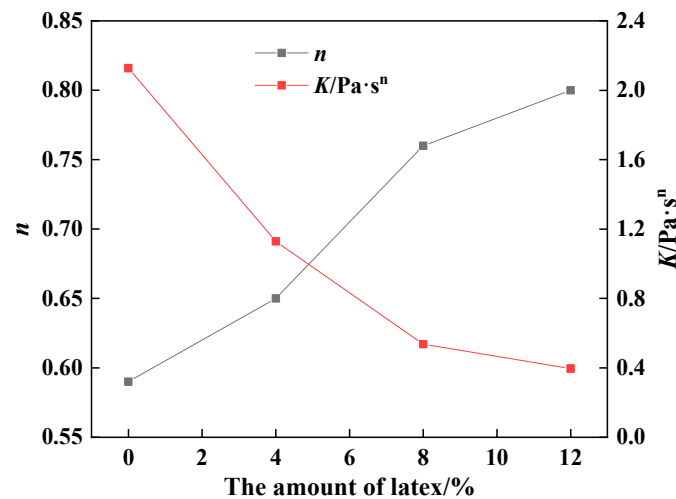
Figure 9. Effect of latex addition on rheological properties of cement slurry.

Table 10 illustrated that, with the increase in the amount of CO_2-corrosion-resistant toughened latex, the free liquid content, the upper and lower density difference of the cement slurry, and the API water loss all showed a downward trend. When the amount of latex added was 8%, the latex significantly enhanced the cement slurry's stability. The cement slurry's free liquid content was currently barely 0.1%, and the difference in density between its top and lower portions is only 0.01 g·cm^{-3}. Concurrently, the cement slurry's water loss decreases to 108 mL from 1150 mL. The results demonstrate that latex may successfully lower the system's water loss. Additionally, latex particles can swiftly spread throughout cement slurry, squeeze out and fill any spaces left by cement particles, and encourage the production of filter cakes. In the meantime, the cement particle surface protection layer creation can help lessen cement particle water loss. As a result, it significantly affects the cement slurry stability and water loss reduction.

Table 10. Effect of latex addition on the stability of cement slurry.

Amount of Latex Added/%	Free Liquid Content/%	Density Difference of Cement Paste/g·cm^{-3}	API Water Loss/mL
0	3.5	0.09	1150
4	0.6	0.03	320
8	0.1	0.01	108
12	0	0	56

The pressurization thickening experiment in Figure 10 showed that the thickening curve of the cement slurry was closer to "right angle thickening" and more stable than that of blank cement following the addition of the CO_2-resistant toughened latex. Indicating that CO_2-resistant toughened latex can still preserve latex properties over time in high-temperature and high-pressure environments and support the rheological stability of the

cement slurry, an increase in the latex content had no discernible impact on the thickening time or consistency. Table 11 showed that the initial and final setting times of the latex cement rose as the latex dose increased. This suggested that latex slowed the hydration of cement, and that the inhibition effect increases as the latex dosage increased. The application of latex particles to the surface of cement particles created a protective film that delayed the hydration reaction time of the cement and had a retarding effect by preventing the cement in the film from coming into contact with water during the hydration induction period and by lowering the reaction's hydration heat [30]. The degree of the latex effect is determined by its charge characteristics and functional group [31]. The anionic functional group on the CO_2-resistant toughened latex's molecular chain gave it a significant adsorption capacity, and lengthened the initial and final setting times.
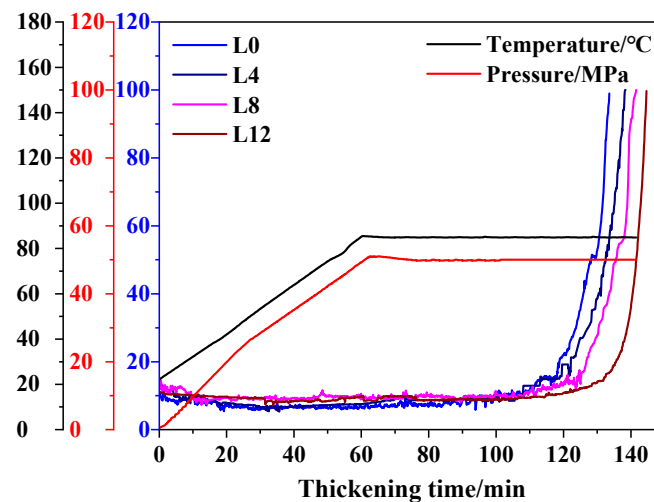

Figure 10. Effect of latex addition on thickening curve.

Table 11. Effect of latex on the setting time of cement slurry.

Amount of Latex Added/%	Initial Setting Time/min	Final Setting Time/min
0	172	213
4	217	272
8	278	343
12	349	391

3.2.2. Effect of Latex on Properties of Cement Composite

Figure 11 illustrated how the compressive and flexural strengths of the latex cement exhibit a tendency of first increasing, and then dropping as the curing time increases. The impact of the latex addition on cement strength likewise exhibited this similar trend. The maximum compressive strength of the latex cement composite was 27.81 MPa, or 13.47% greater than the blank cement composite, when the latex content was 4%. When the amount of latex was 8%, the flexural strength of the latex cement was up to 4.33 MPa, which was 33.64% higher than that of the blank cement, indicating that the latex can be fully dispersed in the cement slurry and form a latex film, and the latex film formed by the latex particles can cover and fill the surface and space of the hydration product. Together with the hydration products, the continuous spatial network structure was formed [32], thereby increasing the physical strength of the cement composite. At the same time, the latex film formed by latex had a lower rigidity and greater flexibility, and had a better improvement effect on the cement composite flexural strength. In addition, because of the requirements of cementing construction, the influence of bubbles produced by emulsifiers in latex cannot be completely eliminated, which led to a decrease in the strength of the cement composite due to the excessive addition of latex.
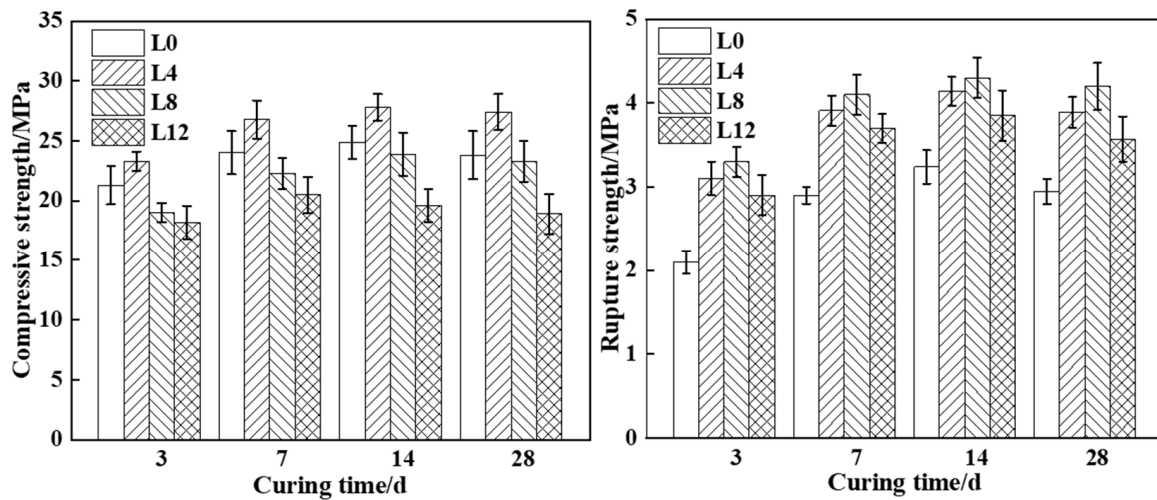
Figure 11. Effect of latex addition on compressive strength and flexural strength of cement.

Figure 12 illustrated the permeability of various cement composites decreased steadily as the curing time increases. The cement's permeability initially rose, and then fell as the amount of latex increases. This demonstrated that the latex can successfully close up remaining holes in the cement composite and raise its density. Simultaneously, the continuous latex coating might lessen the cement permeability by preventing the infiltration of extraneous fluids and strengthening the link between various hydration products.
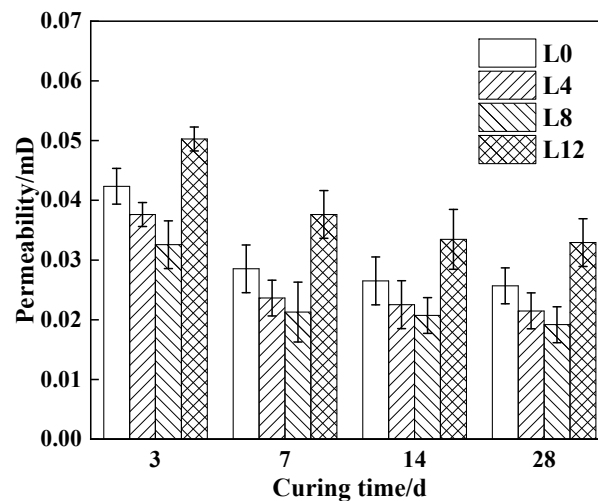
Figure 12. Effect of latex addition on permeability of cement.

3.3. Corrosion Resistance Analysis of CO_2-Resistant Toughened Latex

3.3.1. Effect of Latex on Physical Properties of Cement

As illustrated in Figure 13, as the corrosion time increased, the cement's compressive strength kept decreasing while its permeability gradually increased and changes more quickly over time. The cement can be less susceptible to CO_2 corrosion with the use of CO_2-resistant toughened latex. After 60 days of CO_2 corrosion, the compressive strength of the blank cement system decreased by 27.39% and the permeability increased by 46.88%. However, when the amount of latex was 8%, the compressive strength and permeability of the blank cement system only changed by 11.74% and 19.41%. This demonstrated that the latex film formed by the latex and the filling effect of latex particles effectively protected the hydration products [33], hindered the intrusion of CO_2 into the interior of the cement composite, improved the corrosion resistance of the cement composite, and, thus, slowed the decline in the strength of the cement composite and the increase in permeability.
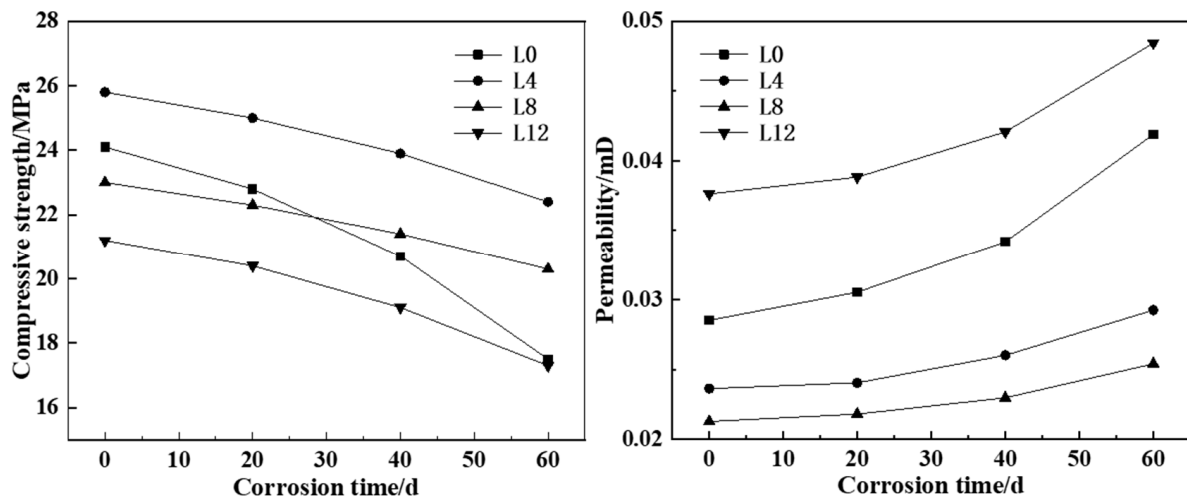
Figure 13. Compressive strength and permeability of cement composite with time.

The surfaces of the cement composite after 60 days of CO_2 liquid-phase corrosion are shown in Figure 14. The surfaces of L0 and L12 were seriously corroded, and numerous corrosion holes and corrosion product $CaCO_3$ were formed, among which the corrosion damage of the blank cement was the most serious, which further led to the acceleration of the CO_2 corrosion rate. However, only a small amount of corrosion occurred on the surface of L4 and L8, and there was no obvious corrosion phenomenon. As Figure 15 illustrates, the corrosion depth of CO_2 on cement tended to rise with increasing corrosion time. The addition of latex can decrease the corrosion depth of CO_2, with the lowest corrosion depth occurring at an 8% latex addition. These all demonstrated that the CO_2-resistant toughened latex's continuous network structure and latex film successfully impeded the eroding effect of CO_2 into the cement composite and the corrosion consumption of alkaline materials. Additionally, Figure 16 showed that the section of the blank cement composite stained by phenolphthalide was continuously reduced as the corrosion time increased. This meant that the non-corroded part of the cement composite gradually decreased until only the central portion remained uncorroded [34], indicating that the CO_2 corrosion of the blank cement composite was extremely serious. The addition of the CO_2-resistant toughened latex can effectively slow down the corrosion rate of CO_2.
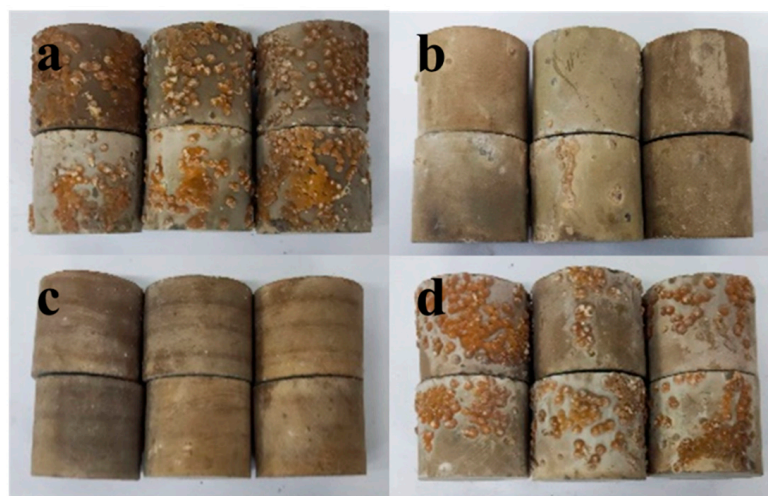

Figure 14. Corrosion diagram of cement surface ((**a**). L0 cement composite, (**b**). L4 cement composite, (**c**). L8 cement composite, and (**d**). L12 cement composite).
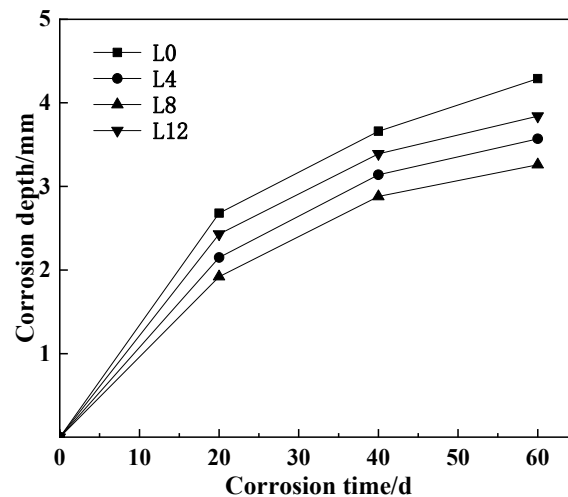
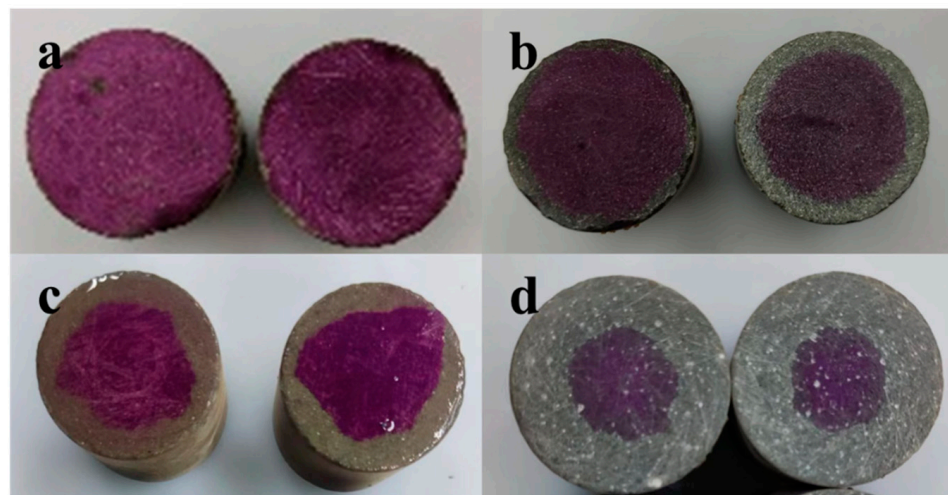**Figure 15.** Corrosion depth of cement composite with time.

Figure 16. The change of corrosion depth of L0 cement composite with time ((**a**). 0 d, (**b**). 20 d, (**c**). 40 d, and (**d**). 60 d).

3.3.2. Effect of Latex on Microstructure of Cement

As per Figure 17, which depicted the physical property change process of the composite and cement, uncorroded cement had a high concentration of amorphous hydrated calcium silicate and $Ca(OH)_2$. The concentrations of the hydrated produced $Ca(OH)_2$ and hydrated calcium silicate will steadily decline as CO_2 corrosion advances and eventually change into carbonated products like calcite $CaCO_3$ and arachite $CaCO_3$ [35]. The consumption of $Ca(OH)_2$ and the subsequent conversion to $CaCO_3$ in the latter stages of corrosion further indicated that significant corrosion was occurring inside the cement composite. In this process, the addition of latex promoted the production of hydration products to a certain extent, and slowed down the corrosion of $Ca(OH)_2$ and the hydrated calcium silicate, indicating that the latex film formed by latex effectively protected the hydration products, blocked the residual pores of cement hydration, reduced the corrosive contact between CO_2 and the hydration products, and improved the corrosion resistance of the cement composite.
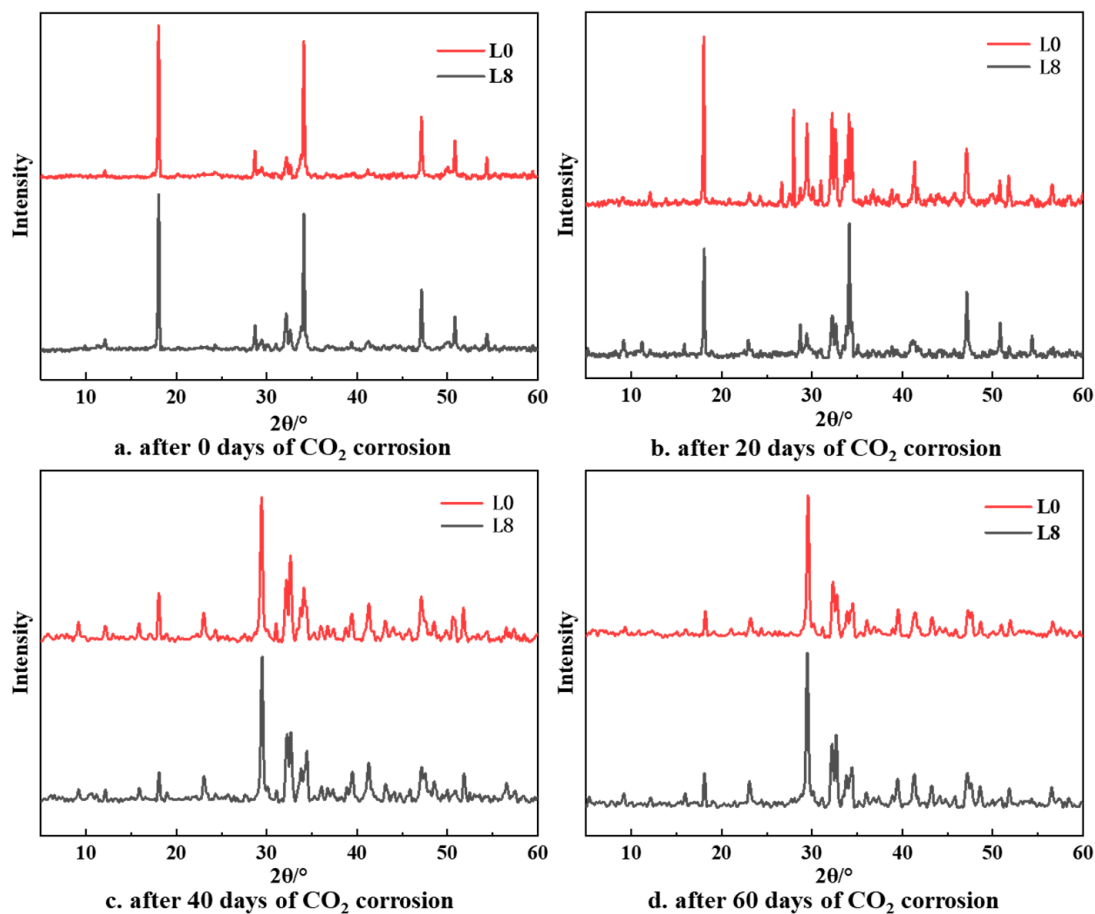
Figure 17. XRD pattern of cement composite after corrosion.

According to the microstructure of the cement composite in Figure 18, it can be found that the cement composite that had been etched for 0 days is still in the hydration reaction. From photo a_1, it can be found that there are flake $Ca(OH)_2$ crystals on the cement composite matrix, needle-etched composite, hydrated calcium silicate clusters gathered and on the surface, and cement clinker particles that have not been completely hydrated. Because of the latex membrane structure, the cement composite matrix that was applied with latex were smoother and more complete, as shown in photo a_2. The latex film also connected the hydration products to produce a more complete cement. The formation of hydrated calcium silicate and $Ca(OH)_2$ was completed by the cement composite with the extension of the corrosion period, producing a more complete form [36]. Simultaneously, the surface of the b_1, c_1, and d_1 cement composite matrix showed signs of corrosion carbonization, and, over time, loose free calcium silicate was progressively created [37,38]. As the corrosion deepens, it was converted into tiny carbonization product $CaCO_3$ particles [39], which caused the strength of the cement composite to rapidly decrease. As compared to the blank cement, the latex cement composite produced far less loose hydrated calcium silicate and carbonization products, and, even after 60 days of corrosion, microcracks will not form on the matrix surface, which suggested that the CO_2-resistant toughened latex can effectively slow down CO_2 corrosion and increase the cement composite's resistance to corrosion.

Figure 19 and Table 12 illustrated that the element composition of the blank cement composite was notably lower in Ca than that of the latex cement composite, with a greater substitution of O. The degree of cement deterioration increased with decreasing calcium concentration [40]. Latex was better at preventing cement from corroding from CO_2 and can effectively slow down the loss of calcium in cement.
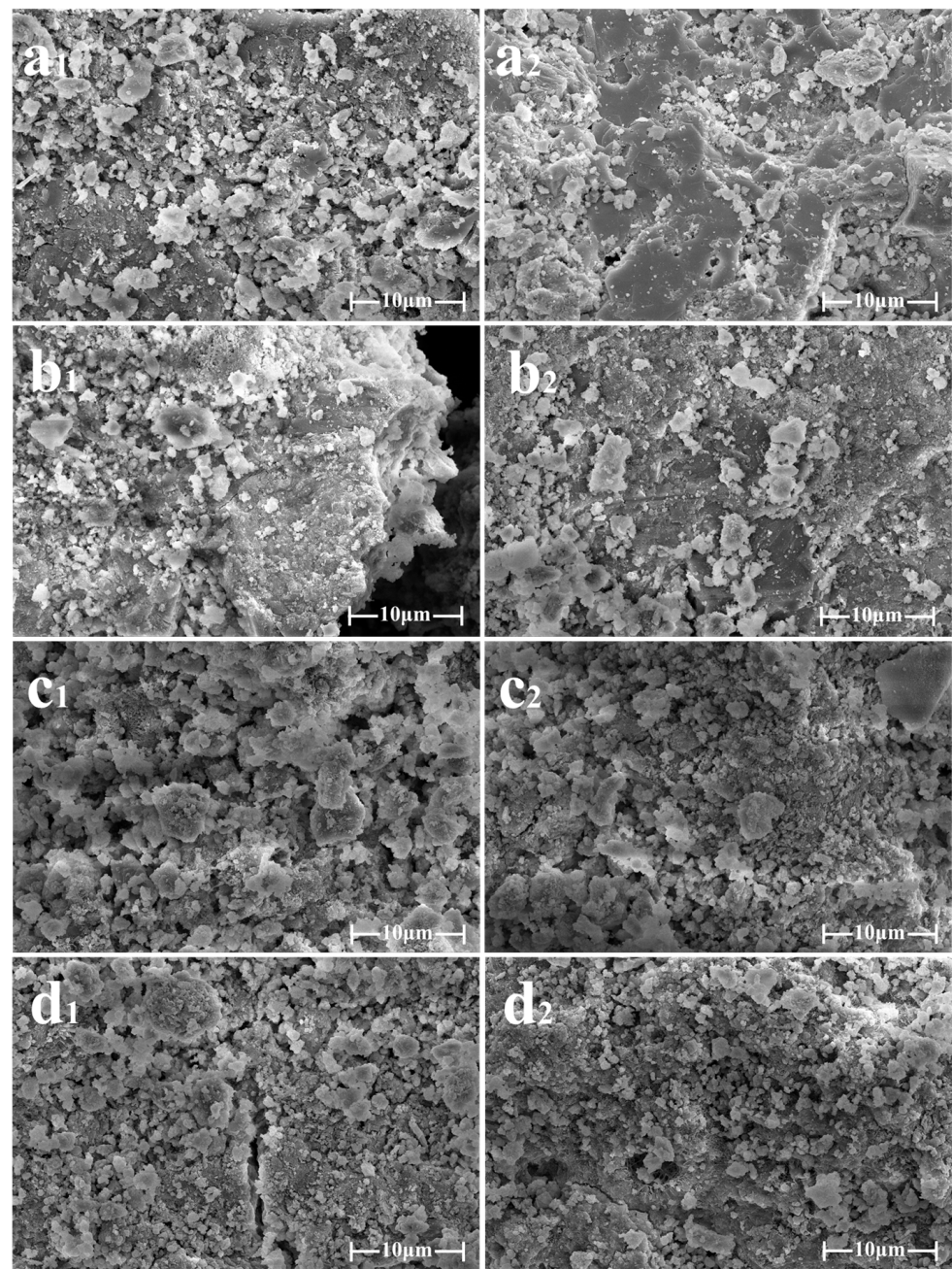
Figure 18. SEM pattern of cement composite after corrosion ((a_1). L0 corrosion for 0 days, (a_2). L8 corrosion for 0 days, (b_1). L0 corrosion for 20 days, (b_2). L8 corrosion for 20 days, (c_1). L0 corrosion for 40 days, (c_2). L8 corrosion for 40 days, (d_1). L0 corrosion for 60 days, and (d_2). L8 corrosion for 60 days).

Table 12. EDX analysis result on hydration products of cement composite.

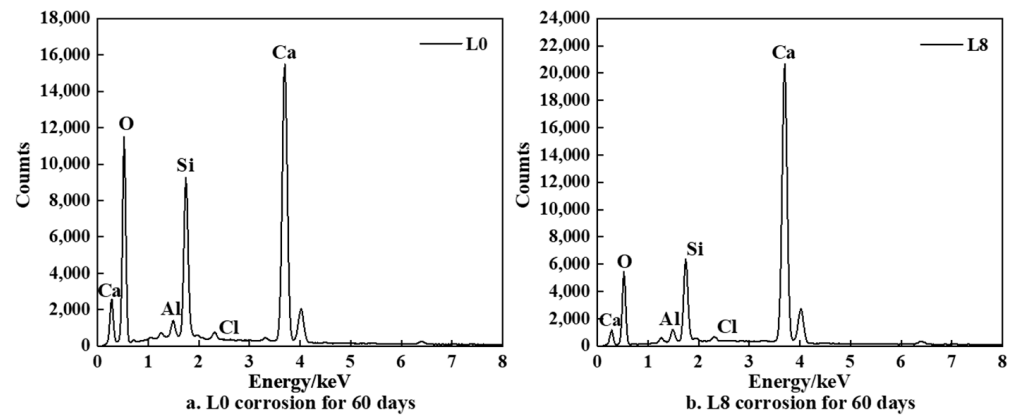| Symbol of Element	L0		L8	
	Weight Percent	**Atom Percent**	**Weight Percent**	**Atom Percent**
O	60.06	77.13	46.99	67.40
Ca	29.14	14.94	44.02	25.21
Si	9.65	7.06	7.63	6.23
Cl	0.05	0.03	0.03	0.02
Al	1.10	0.83	1.34	1.14

Figure 19. EDX of hydration products of cement composite.

3.3.3. Corrosion Resistance Mechanism of CO$_2$-Resistant Toughened Latex

Figure 20 depicted the latex action process on the cement matrix surface. The protective impact of the latex coating and the cementation and filling action of the hydration products were primarily responsible for the system's increased anti-corrosion performance. The latex can more easily disperse on the surface of the cement particles due to its nanoscale particle size. It can also create a continuous latex film in the pores of the cement particles and the surface of the hydration products, which encouraged the development of a continuous network structure between the latex and the hydration products. An improved cement composite density was achieved by covering the pores with a latex film and particles, which inhibited the corrosive medium's penetration and rate of corrosion. Eventually, the cement composite's ability to withstand corrosion was improved.
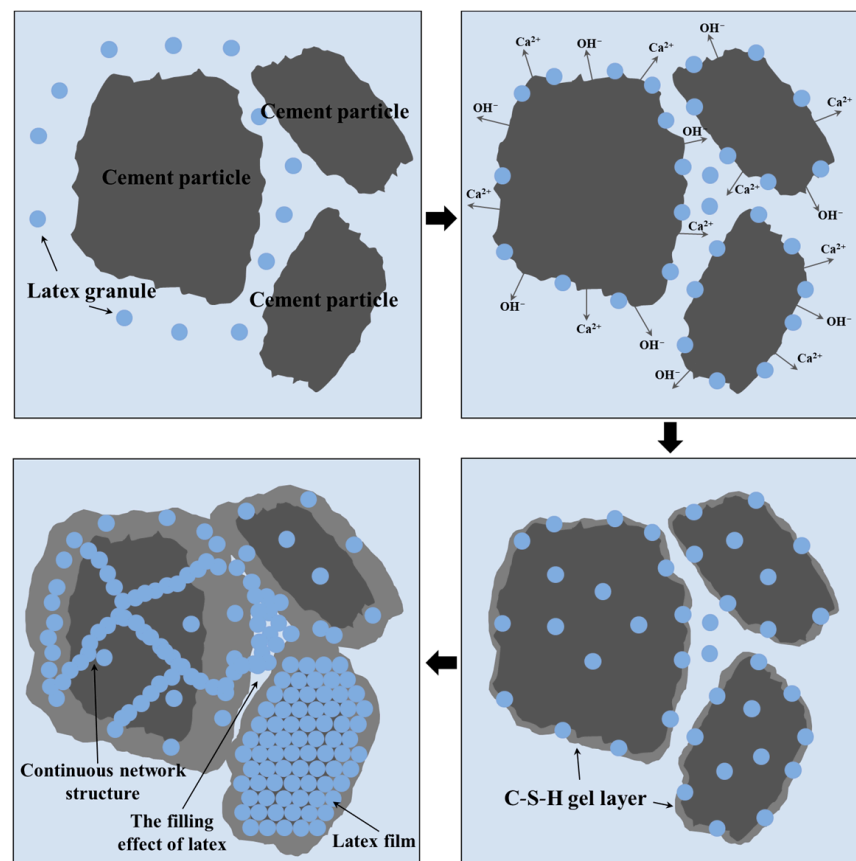

Figure 20. Schematic diagram of latex's anti-corrosion mechanism.

4. Conclusions

In this paper, the CO_2-resistant toughened latex was created using seed emulsion polymerization, using styrene and polybutadiene as the core materials and maleic anhydride, 2-acrylamide, and 2-methylpropanesulfonic acid as the shell materials. Latex had an apparent viscosity of 36.8 mPa ·s, a solid content of 32.2%, and a size distribution that was mostly between 160 and 220 nm. Corrosion-resistant latex had a good mechanical stability, temperature stability, salt stability, and freeze–thaw stability, which was better than ordinary styrene–butadiene latex. In addition to increasing the cement slurry's rheology and stability, latex may also strengthen the cement composite's compressive, flexural, and permeability properties. It can also extend the cement slurry's initial and final setting times and slow down coagulation. When the amount of latex was 8%, the fluidity index of cement slurry was 0.76, the consistency index was 0.5363, the free liquid content was only 0.1%, and the water loss was reduced to 108 mL. The compressive strength and flexural strength of the latex cement composite were increased by 13.47% and 33.64% compared with the blank cement composite.

Then, the corrosion resistance of latex was studied. The findings demonstrated that latex may successfully reduce CO_2 corrosion's rate and effect. At an 8% latex addition, the cement's corrosion resistance was significantly increased, the cement's compressive strength drop rate was lowered from 27.39% to 11.74%, and the permeability growth rate was lowered from 46.88% to 19.41%.

Lastly, the mechanism of resistance to CO_2 corrosion and the change in the latex microstructure during corrosion were examined using XRD and SEM. The film formation and filling effect of latex on hydration products were further analyzed. Latex increased cement's density and reduced the hydration products' corrosion consumption, demonstrating that latex increased cement's resistance to corrosion. According to the experimental findings, the CO_2-resistant toughened latex can significantly improve the physical strength and CO_2 corrosion resistance of the cement, and significantly reduce the influence of CO_2 corrosion on the compressive strength, permeability, and hydration products of the cement. The CO_2-resistant toughened latex can effectively solve the CO_2 corrosion problem of the cementing cement ring and avoid the impact of CO_2 corrosion in shale reservoirs.

Author Contributions: C.J.: writing—original draft, writing—review and editing, and investigation. X.Z. and Y.Z.: data curation, formal analysis, writing—original draft, and writing—review and editing. L.T., Y.L., Z.Z. and H.Z.: conceptualization, funding acquisition, project administration, resources, and methodology. All authors have read and agreed to the published version of the manuscript.

Data Availability Statement: The data are contained within the article.

Conflicts of Interest: Author Lei Tang was employed by the company Sichuan Ruidong Technology Co., Ltd. Author Yuhao Liu was employed by the company CNPC Chuanqing Drilling Engineering Company Limited. Author Zhijun Zhao was employed by the company CNPC Xibu Drilling Engineering Company Ltd., Jundong Drilling Company. The remaining authors declare that the research was conducted in the absence of any commercial or financial relationships that could be construed as a potential conflict of interest.

References

1. Wang, W.; Pang, X.; Wang, Y.; Chen, M.; Chen, Y.; Li, C.; Chen, Z. Hydrocarbon Generation and Residue Features of Ediacaran High-Maturity Source Rocks and Their Significance in Gas Exploration in Sichuan Basin. *Processes* **2023**, *11*, 3193. [CrossRef]
2. Wang, T.; Xu, B.; Chen, Y.; Wang, J. Mechanism and Main Control Factors of CO_2 Huff and Puff to Enhance Oil Recovery in Chang 7 Shale Oil Reservoir of Ordos Basin. *Processes* **2023**, *11*, 2726. [CrossRef]
3. Xia, Z.; Yin, H.; Wang, X.; Xu, G. Surfactant slug assisting CO_2 huff and puff in enhancing shale oil reservoir recovery. *Phys. Fluids* **2024**, *36*, 016601. [CrossRef]

4.   Dai, J.-C.; Wang, T.-Y.; Weng, J.-T.; Tian, K.-J.; Zhu, L.-Y.; Li, G.-S. CO_2 flooding in shale oil reservoir with radial borehole fracturing for CO_2 storage and enhanced oil recovery. *Pet. Sci.* **2023**, *21*, 519–534. [CrossRef]

5.   Dai, J.; Wang, T.; Tian, K.; Weng, J.; Li, J.; Li, G. CO_2 huff-n-puff combined with radial borehole fracturing to enhance oil recovery and store CO_2 in a shale oil reservoir. *Geoenergy Sci. Eng.* **2023**, *228*, 212012. [CrossRef]

6.   Zheng, D.; Miska, S.; Ziaja, M.; Zhang, J. Study of anisotropic strength properties of shale. *AGH Drill. Oil Gas* **2019**, *36*, 93–112. [CrossRef]

7.   Zheng, D.; Ozbayoglu, E.; Miska, S.; Zhang, J. Experimental Study of Anisotropic Strength Properties of Shale. In Proceedings of the 57th U.S. Rock Mechanics/Geomechanics Symposium, Atlanta, GA, USA, 25–28 June 2023.

8.   Zheng, D.; Miska, S.; Ozbayoglu, E.; Zhang, J. *Combined Experimental and Well Log Study of Anisotropic Strength of Shale*; University of Tulsa: Tulsa, OK, USA; British Petroleum P.L.C.: London, UK, 2023.

9.   Kutchko, B.G.; Strazisar, B.R.; Dzombak, D.A.; Lowry, G.V.; Thaulow, N. Degradation of Well Cement by CO_2 under Geologic Sequestration Conditions. *Environ. Sci. Technol.* **2007**, *41*, 4787–4792. [CrossRef]

10.   Abid, K.; Gholami, R.; Choate, P.; Nagaratnam, B.H. A review on cement degradation under CO_2-rich environment of sequestration projects. *J. Nat. Gas Sci. Eng.* **2015**, *27*, 1149–1157. [CrossRef]

11.   Zheng, D.; Ozbayoglu, E.M.; Miska, S.Z.; Liu, Y. Cement Sheath Fatigue Failure Prediction by Support Vector Machine Based Model. In Proceedings of the SPE Eastern Regional Meeting, Wheeling, WV, USA, 18–20 October 2022.

12.   Zheng, D.; Miska, Z.; Ozbayoglu, E.; Zhang, Y. The Influence of Elliptical-Geometry Wellbore on Zonal Isolation. In Proceedings of the 56th U.S. Rock Mechanics/Geomechanics Symposium, Santa Fe, NM, USA, 26–29 June 2022.

13.   García-González, C.A.; el Grouh, N.; Hidalgo, A.; Fraile, J.; López-Periago, A.M.; Andrade, C.; Domingo, C. New insights on the use of supercritical carbon dioxide for the accelerated carbonation of cement pastes. *J. Supercrit. Fluids* **2008**, *43*, 500–509. [CrossRef]

14.   Lesti, M.; Tiemeyer, C.; Plank, J. CO_2 stability of Portland cement based well cementing systems for use on carbon capture & storage (CCS) wells. *Cem. Concr. Res.* **2013**, *45*, 45–54. [CrossRef]

15.   Li, Q.; Lim, Y.M.; Flores, K.M.; Kranjc, K.; Jun, Y.-S. Chemical Reactions of Portland Cement with Aqueous CO_2 and Their Impacts on Cement's Mechanical Properties under Geologic CO_2 Sequestration Conditions. *Environ. Sci. Technol.* **2015**, *49*, 6335–6343. [CrossRef]

16.   Lin, Y.; Zhu, D.; Zeng, D.; Yang, Y.; Shi, T.; Deng, K.; Ren, C.; Zhang, D.; Wang, F. Experimental studies on corrosion of cement in CO2 injection wells under supercritical conditions. *Corros. Sci.* **2013**, *74*, 13–21. [CrossRef]

17.   Morandeau, A.; Thiéry, M.; Dangla, P. Impact of accelerated carbonation on OPC cement paste blended with fly ash. *Cem. Concr. Res.* **2015**, *67*, 226–236. [CrossRef]

18.   Gong, P.; Fu, H.; He, D.; Wu, Y.; Mei, K.; Zhang, C.; He, X.; Liu, T.; Li, S.; Cheng, X. Novel material to enhance the integrity of CCUS cement sheath: Exploration and application of calcium aluminate cement. *Gas Sci. Eng.* **2024**, *124*, 205247. [CrossRef]

19.   Peng, Z.; Lv, F.; Feng, Q.; Zheng, Y. Enhancing the CO_2-H_2S corrosion resistance of oil well cement with a modified epoxy resin. *Constr. Build. Mater.* **2022**, *326*, 126854. [CrossRef]

20.   Zhang, W.; Zheng, C.; Xie, H.; Du, W. Preparation and Application of Self-emulsifying Curing Agent for CO_2 High-Pressure Corrosion-resistant Resin Cement. *Colloids Surf. A Physicochem. Eng. Asp.* **2023**, *680*, 132570. [CrossRef]

21.   Wang, R.; Wang, P.; Li, X. Physical and mechanical properties of styrene-butadiene rubber emulsion modified cement mortars. *Cem. Concr. Res.* **2005**, *35*, 900–906. [CrossRef]

22.   Wang, M.; Wang, R.; Zheng, S.; Farhan, S.; Yao, H.; Jiang, H. Research on the chemical mechanism in the polyacrylate latex modified cement system. *Cem. Concr. Res.* **2015**, *76*, 62–69. [CrossRef]

23.   Eren, F.; Gödek, E.; Keskinateş, M.; Tosun-Felekoğlu, K.; Felekoğlu, B. Effects of latex modification on fresh state consistency, short term strength and long term transport properties of cement mortars. *Constr. Build. Mater.* **2017**, *133*, 226–233. [CrossRef]

24.   Jiang, M.; Zheng, Z.; Ding, X.; Cheng, X.; Peng, Y. Convenient synthesis of novel fluorinated polyurethane hybrid latexes and core-shell structures via emulsion polymerization process with self-emulsification of polyurethane. *Colloid Polym. Sci.* **2007**, *285*, 1049–1054. [CrossRef]

25.   Protonotariou, S.; Evageliou, V.; Yanniotis, S.; Mandala, I. The influence of different stabilizers and salt addition on the stability of model emulsions containing olive or sesame oil. *J. Food Eng.* **2013**, *117*, 124–132. [CrossRef]

26.   Ghosh, S.; Cramp, G.L.; Coupland, J.N. Effect of aqueous composition on the freeze-thaw stability of emulsions. *Colloids Surf. A Physicochem. Eng. Asp.* **2006**, *272*, 82–88. [CrossRef]

27.   Xu, Y.; Li, P.; Liu, M.; Yu, Y.; Guo, J. Synthesis, performance and working mechanism of a novel amphoteric polycarboxylate dispersant without chlorine ion. *Constr. Build. Mater.* **2020**, *247*, 118613. [CrossRef]

28.   Yang, Y.; Yuan, B.; Wang, Y.; Zhang, S.; Zhu, L. Carbonation resistance cement for CO_2 storage and injection wells. *J. Pet. Sci. Eng.* **2016**, *146*, 883–889. [CrossRef]

29.   Zhao, J.; Hu, M.; Liu, W.; Feng, J.; Zhang, H.; Liu, M.; Guo, J. Toughening effects of well-dispersed carboxylated styrene-butadiene latex powders on the properties of oil well cement. *Constr. Build. Mater.* **2022**, *340*, 127768. [CrossRef]

30.   Kong, X.; Emmerling, S.; Pakusch, J.; Rueckel, M.; Nieberle, J. Retardation effect of styrene-acrylate copolymer latexes on cement hydration. *Cem. Concr. Res.* **2015**, *75*, 23–41. [CrossRef]

31.   Lu, Z.; Kong, X.; Zhang, C.; Xing, F.; Cai, Y.; Jiang, L.; Zhang, Y.; Dong, B. Effect of surface modification of colloidal particles in polymer latexes on cement hydration. *Constr. Build. Mater.* **2017**, *155*, 1147–1157. [CrossRef]

32. Cheng, X.; Chen, Z.; Gu, T.; Zeng, L.; Yao, L.; Chen, Z.; Huang, K.; Zhang, Z.; Zhang, C.; Liu, K.; et al. Study on the dynamic and static mechanical properties of microsphere rubber powder reinforced oil well cement composites. *Constr. Build. Mater.* **2021**, *309*, 125145. [CrossRef]

33. Xu, B.; Yuan, B.; Wang, Y.; Zeng, S.; Yang, Y. Nanosilica-latex reduction carbonation-induced degradation in cement of CO_2 geological storage wells. *J. Nat. Gas Sci. Eng.* **2019**, *65*, 237–247. [CrossRef]

34. de Sena Costa, B.L.; de Oliveira Freitas, J.C.; Silva Santos, P.H.; de Arau'jo Melo, D.M.; Gomes da Silva Araujo, R.; de Oliveira, Y.H. Carbonation in oil well Portland cement: Influence of hydration time prior to contact with CO_2. *Constr. Build. Mater.* **2018**, *159*, 252–260. [CrossRef]

35. Gruyaert, E.; VandenHeede, P.; DeBelie, N. Carbonation of slag concrete: Effect of the cement replacement level and curing on the carbonation coefficient—Effect of carbonation on the pore structure. *Cem. Concr. Compos.* **2013**, *35*, 39–48. [CrossRef]

36. Zárybnická, L.; Pokorný, J.; Machotová, J.; Ševčík, R.; Šál, J.; Viani, A. Study of keto-hydrazide crosslinking effect in acrylic latex applied to Portland cements with respect to physical properties. *Constr. Build. Mater.* **2023**, *375*, 130897. [CrossRef]

37. Duguid, A.; Scherer, G.W. Degradation of oilwell cement due to exposure to carbonated brine. *Int. J. Greenh. Gas Control.* **2010**, *4*, 546–560. [CrossRef]

38. Duguid, A.; Radonjic, M.; Scherer, G.W. Degradation of cement at the reservoir/cement interface from exposure to carbonated brine. *Int. J. Greenh. Gas Control.* **2011**, *5*, 1413–1428. [CrossRef]

39. Zhang, Y.; Xu, M.; Song, J.; Wang, C.; Wang, X.; Hamad, B.A. Study on the corrosion change law and prediction model of cement stone in oil wells with CO_2 corrosion in ultra-high-temperature acid gas wells. *Constr. Build. Mater.* **2022**, *323*, 125879. [CrossRef]

40. Phung, Q.T.; Maes, N.; Jacques, D.; De Schutter, G.; Ye, G.; Perko, J. Modelling the carbonation of cement pastes under a CO_2 pressure gradient considering both diffusive and convective transport. *Constr. Build. Mater.* **2016**, *114*, 333–351. [CrossRef]